JAAS
Journal of Analytical Atomic Spectrometry

Accepted Manuscript

This article can be cited before page numbers have been issued, to do this please use: G. Liu, T. Ulrich, F. Xia and Y. Xiao, *J. Anal. At. Spectrom.*, 2023, DOI: 10.1039/D2JA00341D.

View Article Online
DOI: 10.1039/D2JA00341D

Brama： a new freeware Python software for reduction and imaging of LA-ICP-MS data from U-Pb scans

Guoqi Liu*[a], Thomas Ulrich [b], Fei Xia [a], Yang Xiao [c]

[a] State Key Laboratory of Nuclear Resources and Environment, East China University of Technology, Nanchang, 330013, China.

[b] Department of Geoscience, Aarhus University, Høegh-Guldbergs Gade 2, DK-8000 Aarhus C, Denmark.

[c] Sichuan Chuangyuan Microspectrum Technology Co., Ltd., Chengdu 610300, China.

* Corresponding author, E-mail address: liuguoqi@ecit.edu.cn (G.-Q. Liu)

View Article Online
DOI: 10.1039/D2JA00341D

Abstract: U-Pb dating of hydrothermal and hydrothermal accessory minerals is challenging because they often contain high concentrations of common Pb, low U concentrations, and they can be altered and fractured. Photomicrography, Bayesian regression, and trace element and isotope ratio maps have effectively been used to overcome these problems in dating such minerals. A new software, Brama (Bayesian Regression and Age Mapping Application) for LA-ICP-MS U-Pb data, performs outlier processing, baseline correction, isotope calculation and Bayesian regression by matching the laser ablation position of the line scan with the time-resolved signal of the plasma mass spectrometry data generated from quadrupole instruments, resulting in high resolution spatial maps of trace element and isotope ratios as well as age results. The software-derived data can also be used in the Tera-Wasserburg and Wetherill methods to calculate mineral ages. We demonstrate the key advantages and potential applications of Brama with two examples of LA-ICP-MS calcite and apatite U-Pb dating.

Keywords: U-Pb dating; Imaging; Python software; Bayesian regression

1. Introduction

U-Pb dating of hydrothermal accessory minerals is of great importance for petrology and ore deposit research.[1-3] The *in-situ* quadrupole LA-ICP-MS analysis technique provides an economical and efficient way of U-Pb dating. However, factors such as low U content, high concentrations of initial Pb, inclusions and fractures in some of these minerals hinder the extraction of true isotopic U-Pb age information.[4] More accurate ages have recently been obtained from LA-ICP-MS trace element or isotope ratio maps as well as photomicrographs to filter the data for U-rich or unaltered regions.[4-6] Therefore, the processing of low count data and the acquisition of the spatial distribution of elemental or isotope ratio data is essential for U-Pb dating. Davis and Rochín-Bañaga (2021) proposed a Bayesian regression approach and released the VBA-based Excel program Utilchron.[7] Although the Utilchron regressions were successful in obtaining ages for fossils and calcite, the data import and laser analysis position coordinate matching could not be done automatically.[2,8] Iolite provides a powerful framework for processing mass spectrometric data, and performs downhole fractionation corrections by data reduction scheme in combination with the ^{207}Pb or ^{208}Pb method for the calibration of common Pb in standards.[10,11] Iolite is widely used in processing data for single point ablation or line scans of

View Article Online
DOI: 10.1039/D2JA00341D

regular variations of U/Pb isotopes. Hydrogenic and fossil material often contains low U levels and variable amounts of common Pb, and therefore, requires processing of large amounts of individual low-count data from line scans. [7] In Iolite it is not possible to filter and interpolate such data as well as to estimate age using Bayesian regression. Here, we present Brama (Bayesian Regression and Age Mapping Application) for LA-ICP-MS U-Pb dating data, which is an open-source and user-friendly Python program focused on processing the isotope ratios for each detection cycle to obtain high-resolution isotope ages on the time series scale. Brama can automatically match and segment continuously acquired mass spectrometry data. The software can also perform spike filtering, standard bias correction, interpolation, filtering for counting, batch processing of multiple files and Bayesian regression calculations. Finally, Brama enables the mapping of isotope and spatial distribution of age data. To demonstrate these features of the software, two examples of hydrothermal mineral dating are provided in this paper.

2. Line scan versus point analysis

Point and line ablation analysis are the two basic ways of sampling by LA-ICP-MS. Generally, the isotope ratios and errors are calculated by averaging the U-Pb isotope counts detected by the mass spectrometer during the ablation for the same site or for continuous ablation sampling along the path. The mixing of the mineral's common Pb yields widely varying U-Pb isotope ratios, and the averaging method may cause deviation from the true value. In order to discuss the influence of the averaging method and the individual treatment of each data on the dating results, we simulate a mineral U-Pb isotope model (The simulation method is described in the supporting information). We use two indicators to judge the simulation results: one is the approximate degree of the simulation result age and the real age (100 Ma), and the other is the error value of the age. Closer to the real age or smaller age errors indicate a good simulation. The python script file for the simulation program can be downloaded from https://github.com/sndjgm/U-Pb-isotope-simulation-and-sampling.

2.1 Simulation to analyze the effect of spatial resolution on the error of the age determination

In our simulation we assume that the U-Pb age of the mineral is 100 Ma and that it contains different proportions of common Pb at the time of its U-Pb isotope closure. The ^{206}Pb counts were set to vary

View Article Online
DOI: 10.1039/D2JA00341D

from 100 to 1000 in a mineral area of 30 × 33 length units. The ^{207}Pb counts, ^{238}U counts, $^{207}Pb/^{206}Pb$, $^{238}U/^{206}Pb$ and proportion of common Pb are distributed within this area as shown in Fig. 1a. The U-Pb content and isotopic ratios of minerals formed at 100 Ma are spatially unevenly distributed due to the mixing of common Pb. We specify a 1×1 unit area as the basic unit, with a homogeneous U-Pb content and isotope ratio. Without considering the analytical error, the obtained U-Pb isotope results fall on the line with the function y=-0.01242x+0.842 (determined by age=100Ma and initial Pb=0.842) on the Tera-Wasserburg diagram (Fig. 1b, c) irrespective of the sampling mode (point or lines). When we increase the sampling area to 2×2 the lower intercept age obtained by point sampling is 100 ± 5.8 Ma (n=8), while the lower intercept age obtained by the line sampling is 100 ± 2.1 Ma (n=30). When the sampling area is 3×3, the lower intercept age obtained by the point measurement is 100 ± 5.8 Ma (n=8) and the lower intercept age obtained by the line scan is 100 ± 2.8 Ma (n=30). The above results show that the errors of the age obtained in the point and line patterns increase as the sampling beam spot increases. However, when using line sampling, the error increases less than using the point ablation sampling mode when the beam spot is increased.

2.2 Simulation of the effect of possible factors on age results

In reality, the ratio of common Pb, elemental content, and analytical errors exist and vary randomly. Therefore, it is necessary to simulate the effect of the influencing factors (such as common Pb mixing, content-limited analytical error and the number of samples and their locations) on the results of point and line scan analyses. First, we determine the influencing factors and the random distribution model. Subsequently, we use the random sampling method to sample the point analysis and the line scan analysis respectively, and finally we analyze the sampling results. Because the mixing of common Pb is random and the probability distribution model is uniform, the proportion of common Pb mixed, is randomly selected between 0 and 99%. The analytical errors of ^{206}Pb, ^{207}Pb and ^{238}U are positively correlated with the number of counts, so the errors need to be set separately according to their counts. Here we assume an error of 25 % for ^{206}Pb counts below 10, an error of 10 % for ^{206}Pb counts between 10 and 30, and a 3 % error for ^{206}Pb counts greater than 30. These numbers are based on the daily signal monitoring of standards over an extended period of 45 days (Table S2). Daily signal monitoring

View Article Online
DOI: 10.1039/D2JA00341D

of standards in our laboratory shows that errors below a few tens of counts for ^{206}Pb are greater than 23%, while the error is close to 2% for counts greater than a million. Because complex factors such as laser ablation conditions and detector's sensitivity affect the error, it is impossible to accurately estimate the analytical error. Nevertheless, the random distribution model of analysis error conforms to the Poisson distribution, so the Poisson distribution error values are randomly selected according to the elements content. Based on the above random factor settings, a spatial data model with an area of 100*100 units is constructed, which contains the simulated analysis point coordinates, isotope counts, isotope ratios and errors (Fig. 2). In order to simulate the actual analysis process of point and line scan analysis, different numbers of point and line data are randomly selected by a random sampling method. The results of the point and line scan patterns are shown in Table 1 and Fig. S2. The point and line scan analysis models yielded smaller age errors as the laser spot size and U content (or ^{206}Pb, ^{207}Pb and ^{238}U counts) increases (Fig. 2). Compared with the point analysis mode, the age obtained by the line scan mode is more stable under different lengths and positions of the line scan sampling conditions (Fig. 2). The error on the age obtained from point analysis becomes smaller as the number of analysis points increases (Fig. 2). The accuracy and error of the age in the point analysis are influenced by both the number of sampling points and the U content, while in the line scan patterns, they are mainly influenced by the U content. From the simulation of sampling only, the line scan analysis has better stability and accuracy than the point analysis.

2.3 Advantages and disadvantages of line vs. spot analysis

Point analysis can yield the age of small grains of minerals, with tens of seconds of continuous analysis at a single location to obtain accurate isotope ratios. Nevertheless, down-hole fractionation effects will affect the U-Pb ratios and need to be corrected.[10-11] In addition, when the analysis spot is located in a region of low U content, it will result in a large analysis error.

Line scan analysis is suitable for large mineral grains (> 1 mm). Because the line scan ablates on the mineral surface only, down-hole fractionation is negligible. Ablation along a specified path generates hundreds of U-Pb isotope data points that can be link to the ablation sites along the line. Furthermore, the age data obtained from line scan sampling have better stability and accuracy compared to point

View Article Online
DOI: 10.1039/D2JA00341D

analysis (see above). At present, most of the U-Pb dating data processing software is used to average time slices of point or line scan analysis, and only Utilchron is available to process individual data from line scan by interpolation method. Here we present a new python program to filter spikes and counts, interpolate and correct standard bias fracionation for line scan dating processing that uses Bayesian regression.

3. Data reduction process

3.1 Software workflow

The functions of the Brama software include data matching, isotope ratio calculation, age regression calculation, isotope and age distribution mapping (Fig. 3).

3.2 Data matching

Brama can use either single files containing continuous signal intensity streams and laser log files to match, or signal intensity stream files with sample split files. The software supports mass spectra and laser log files in .csv format generated by different quadrupole ICP-MS instruments. For multiple sample processing or age distribution mapping, continuous signal data need to be segmented and matched with the position and timestamp information in the laser log file (Details can be found in supporting information- User Manual of Brama v2.0).

3.3 User interface

As shown in Fig. 4, the Brama interface is divided into seven zones:

(1) *Directory environment setting:* Splits multiple files and single files can be imported by setting the mass spectrometry file, List file and save directory.

(2) *Instrument model selection:* Brama can automatically import data from Agilent and Thermo ICP-MS instrument. Other instrument data can be imported by modifying the table header and format, or we can add more instrument formats based on user feedback.

View Article Online
DOI: 10.1039/D2JA00341D

(3) *Parameter setting:* This area contains parameter settings for standard bias fractionation factor, dwell time, fractionation correction, baseline correction, and outlier filtering.

(4) *Regression setting:* Bayesian regression is performed as one of the choices to obtain age and common Pb ratios. This zone sets the Bayesian regression age, common Pb range, and outlier filtering thresholds.

(5) *Multi-file processing:* This zone provides batch calculations for multiple samples or multiple line scans with the same measurement conditions.

(6) *Mapping processing*: This function merges the result batch line files from step 5 to make isotope and age distribution maps.

(7) *Information:* This window displays the run status, error messages, and results.

3.4 Age regression calculation

Conventional least-squares regression of ratios on the Wetherill and Tera-Wasserburg plot is used for the U-Pb age calculation. The Bayesian approach is used to process low-counts data and to regress count rates in a 3D space.[7] The "*_Results.xls" file generated by Brama contains data columns for the Wetherill and Tera-Wasserburg regressions, which allow for age and common Pb calculations by Isoplot.[13] A Bayesian regression approach can be used to obtain age and initial common Pb isotopic ratios.[7] The square of weighted deviations (SWD) of each datum compared to the best-fit surface is used to filter data that is significantly deviating from the regression. The SWD filtered data is saved as a "*_regress_Result.xls" file. Prior to the isotope and age distribution mapping, the isotope calculation should be done for single or multiple files. Although the age distribution mapping is only meaningful for samples with concordant ages, Brama can present the spatial distribution of all U-Pb isotope ratios and concentrations.

4. Applications

As an illustration of the main features of the software and to show its effectiveness, we used simulated data, as well as calcite and apatite dating analysis.

View Article Online
DOI: 10.1039/D2JA00341D

4.1 Simulated data for verification

Using the simulation software and data presented in Section 2.2 of this paper, a table of 10,000 U-Pb isotopic compositions was constructed. These data are derived from an age of 100 Ma, mixed with different proportions of common Pb and with analytical errors according to the U content. The data with U < 5 cps (counts per second) were filtered, and 9633 data were obtained for age regression calculation. Bayesian regression yielded an age of 100.3 ± 0.75 Ma and a $^{207}Pb/^{206}Pb$ ratios of 0.8388 ± 0.0072. The Tera-Wasserburg and Wetherill regression give similar results (Fig. S3).

To validate Brama in dealing with U-Pb counts and age distribution mapping, we simulated 100 rows × 100 columns of common Pb-free U-Pb isotope data (Fig. S4 a, b). The characteristics of the 10,000 simulated data generated are shown in Table 2. The simulation data were batch processed by the Brama software, and the results of the simulated data processed by Brama are consistent with the model of simulation (Fig. S4; Table 2).

4.2 Calcite dating

Calcite U-Pb dating was performed using a Thermo Scientific quadrupole iCap TQ inductively coupled plasma mass spectrometry (Q-ICP-MS) and an ASI Resolution LR 193 nm ArF excimer laser ablation (LA) system at Sichuan Chuanyuan Weipu Analytical Technology Co. Ltd. The data were collected using line scans on samples and standards. The line scanning speed is 20 μm s^{-1} with total length of 3-4 mm (laser fluence of 3.5J cm^{-2}, frequency of 15 Hz and spot size of 120 μm). Glass standards NIST614 and WC-1 were used to correct for mass fractionation bias between each measurement.[14]

As shown in Fig. 5, the in-house secondary calcite standard AHX yields an age of 235.4 +1.27 /- 1.26 Ma (N=774, MSWD=2.91) by Bayesian regression. The Tera-Wasserburg regression gives similar results (Fig. 5a-d). Data rejection based on U counts (Fig. 5c) or SWD (Fig. 5d) yielded essentially the same ages. The initial common Pb ratios obtained by these two methods are also quite similar. Brama also gives the spatial distribution of isotope counts (Fig. 5c). This can reveal any

View Article Online
DOI: 10.1039/D2JA00341D

relationship between outliers in the sample and its structure. Despite the heterogeneous elemental content of the AHX sample, the isotopes maintain the same trend and give the same formation time.

4.3 Apatite dating

LA-ICP-MS apatite U-Pb dating with line scans was carried out at the Department for Geoscience, University of Aarhus using an Agilent 7900 ICP-MS connected to a 193 nm ArF excimer laser ablation system (Resolution-S155). The sample is embedded in epoxy resin and analyzed using a spot size of 60 µm, scanning speed of 15 µm s^{-1}, fluence of 4J cm^{-2} and repetition rate of 10 Hz. Glass standards NIST614 and matrix-matched apatites MAD1 and BRZ were used to correct for mass fractionation bias between each measurement. MAD1 has an ID-TIMS age of 486.6 ± 0.9 Ma [15] while BRZ-1 has an ID-TIMS age of 2052 ± 1.7 Ma.[16]

The U/Pb ratios for MAD1 and BRZ are too radiogenic and have too little spread to define precise initial isotopic common Pb ratios (Fig. 6). Therefore, ages were calculated after fixing the initial $^{207}Pb/^{206}Pb$ ratios at average crustal values modeled by Stacey and Kramers, which are 0.869 for MAD1 and 1.01 for BRZ-1.[9] As shown in Fig. 6, the MAD1 apatite [15] yields an age of 486.0 +8.8/-10.9 Ma (N=123, MSWD = 2.28, Fig. 11a) using the Bayesian approach, which is similar to the intercept age from the Tera-Wasserburg regression (487.2 ± 6.1 Ma, Fig. 6b). The BRZ-1 apatite gives an age of 2032 +14/-16 Ma (N=1164, MSWD = 2.46, Fig. 6c) by Bayesian regression and 2063 ± 6.4 Ma (MSWD=0.27; n=1164, Fig. 6d) by Tera-Wasserburg regression. These results are consistent with the ID-TIMS ages (Fig. 6).[15-16]

Conclusions

The Python program Brama can successfully extract high-resolution U-Pb isotope information and determine isotopic ages by multiple regression methods. Brama has a user-friendly interface and exports data in formats that other software can access. The software can import data from multiple quadrupole mass spectrometers and link to laser file data. In addition, the software provides a Bayesian regression approach to calculate the age and export the results. Finally, this software is open-source and can provide a foundation for extensions and further developments by scholars familiar with

View Article Online
DOI: 10.1039/D2JA00341D

programming. This software is free for students and researchers and can be requested from the first author. Users can also download the source code directly from https://github.com/sndjgm/Brama.

Windows users can download the exe package file from the following URL:

http://pan.ecut.edu.cn:80/link/F2F1BCCC219B83D15AB0756CA9B3234D

Author Contributions

Guoqi Liu, conceptualization, formal analysis, methodology, software, writing - original draft, writing – review & editing; Thomas Ulrich, formal analysis, methodology, writing – review & editing. Yang Xiao, resources, formal analysis, methodology; Fei Xia, resources, investigation, writing – review & editing.

Conflicts of interest

There are no conflicts to declare.

Acknowledgements

This research was supported by the National Natural Science Foundation of China (No. 41862010 and 42172098). The work of Guoqi Liu at Aarhus University was supported by the China Scholarship Council (202008360007). Constructive discussions with Donald W. Davis have greatly improved the paper. This manuscript benefited from detailed reviews.

References

1. L. A. Neymark, C. S. Holm-Denoma and R. J. Moscati, *Chem. Geol.*, 2018, **483**, 410-425. DOI: 10.1016/j.chemgeo.2018.03.008.

2. H. Rochín-Bañaga, D. W. Davis and T. Schwennicke, *Geology.*, 2021, **49**, 1027-1031.

3. P. Yang, G. Wu, P. Nuriel, A. D. Nguyen, Y. Chen, S. Yang, Y.-x. Feng, Z. Ren and J.-x. Zhao, *Chem. Geol.*, 2021, **568**, 120125.

4. K. Drost, D. Chew, J. A. Petrus, F. Scholze, J. D. Woodhead, J. W. Schneider and D. A. T. Harper, *Geoc., Geop., Geos.*, 2018, **19**, 4631-4648.

5. G. Hoareau, F. Claverie, C. Pécheyran, C. Paroissin, P.-A. Grignard, G. Motte, O. Chailan and J.-P. Girard, *GChron.*, 2020.

View Article Online
DOI: 10.1039/D2JA00341D

6. N. M. W. Roberts, K. Drost, M. S. A. Horstwood, D. J. Condon, D. Chew, H. Drake, A. E. Milodowski, N. M. McLean, A. J. Smye, R. J. Walker, R. Haslam, K. Hodson, J. Imber, N. Beaudoin and J. K. Lee, *GChron.*, 2020, **2**, 33-61

7. D. W. Davis and H. Rochín-Bañaga, *Chem. Geol.*, 2021, **582**, 120454.

8. G. R. Dix, D. W. Davis, K. Chadirji-Martinez, D. D. Marshall, J. L. Kendrick, C. Yakymchuk and C. N. Sutcliffe, *Chem. Geol.*, 2021, **586**, 120582.

9. J. t. Stacey and J. Kramers, *Earth. Planet. Sc. Lett.*, 1975, **26**, 207-221.

10. D. M. Chew, J. A. Petrus and B. S. Kamber, *Chem. Geol.*, 2014, **363**, 185-199.

11. C. Paton, J. D. Woodhead, J. C. Hellstrom, J. M. Hergt, A. Greig and R. Maas, *Geochem., Geophys., Geosyst.*, 2010, **11** (3).

12. C. Paton, J. Hellstrom, B. Paul, J. Woodhead and J. Hergt, *J. Anal. At. Spectrom.*, 2011, **26**, 2508-2518.

13. K. R. Ludwig, *Geochim. et Cosmochim. AC.*, 1998, **62**, 665-676.

14. N. M. W. Roberts, E. T. Rasbury, R. R. Parrish, C. J. Smith, M. S. A. Horstwood and D. J. Condon, *Geochem., Geophys., Geosyst.*, 2017, **18**, 2807-2814.

15. S. N. Thomson, G. E. Gehrels, J. Ruiz and R. Buchwaldt, *Geochem., Geophys., Geosyst.*, 2012, **13**, 1-23.

16. F. E. Apen, C. J. Wall, J. M. Cottle, M. D. Schmitz, A. R. C. Kylander-Clark and G. G. E. Seward, *Chem. Geol.*, 2022, **590**, 120689.

View Article Online
DOI: 10.1039/D2JA00341D

Table1 Results of line scan and point pattern U-Pb isotope age simulations.

Num. of Data	point pattern			Line scan pattern		
	U （Counts）	Age (Ma)	MSWD	U （Counts）	Age (Ma)	MSWD
25	12~182	96.6±7.3	1.03	6~191	99.2±6.2	0.39
	94~1174	99.6±3.5	0.47	76~1175	99.5±4.0	0.51
	15~3527	98.4±3.6	0.44	48~3936	100.26±0.57	0.42
50	15~4772	99.7±1.5	0.44	18~3652	100.33±0.66	0.4
75	15~4920	100.03±0.71	0.48	18~2340	99.86±0.85	0.4
100	8~6128	100.30±0.79	0.42	18~5200	100.27±0.52	0.47
	39~5972	99.72±0.50	0.58	12~5132	100.35±0.55	0.43

Table 2 Comparison of simulated data and results of simulated data with Brama line scan method.

		^{206}Pb (cps)				^{207}Pb (cps)				^{238}U (cps)				^{206}Pb/^{238}U Age (Ma)		
Zone	Num.	Average	Min.	Max.	SD	Average	min	max	SD	Average	min	max	SD	Mean	±2δ	MSWD
Simulated data characteristics																
1			0.12	50			0.13	2.49			0.29	3276		100	0.00	0.00
2			5.3	100			0.24	4.83			350	7245		90	0.00	0.00
3			2.8	50			0.13	2.50			214	4140		80	0.00	0.00
4			0.80	3.0			0.04	0.16			68	297		70	0.00	0.00
5			0.01	0.24			0.01	0.24			0.01	0.49				
Results of simulated data by Brama processing																
1	320	27	2.8	92	15.7	1.28	0.13	4.4	0.8	1724	177	6529	1060	99.9	0.4	0.55
2	954	68	2.8	100	19.3	3.25	0.14	4.8	0.9	4848	229	7245	1368	89.8	0.1	0.75
3	1578	25	0.90	89	14.4	1.21	0.04	4.3	0.7	2034	83	6282	1135	80.0	0.1	0.95
4	2218	2.1	0.01	44	2.5	0.10	0.02	2.0	0.1	187	0.02	3489	198	70.1	0.3	0.22
5	4818	0.13	0.01	2.8	0.1	0.13	0.01	0.24	0.1	0.74	0.01	265.74	10.06			

View Article Online
DOI: 10.1039/D2JA00341D

Figure captions

Fig. 1 (a) Spatial distribution relationships of U-Pb isotopes and contents due to common Pb mixing under the ideal model. The data resolution is 33 x 30 pixels, with no error in individual pixel spot. The circles containing A-H indicate the sampling position for point sampling, and the transparent rectangles indicate the position for line sampling. (b ~ c) Tera-Wasserburg diagrams demonstrating the errors caused by sampling point and line scan patterns under different "beam spot" conditions. The larger the beam spot, the larger the error caused by the "average" data points. Using the same "beam spot", the line scan mode sampling causes a significantly smaller error than the point mode.

Fig. 2 Plot of simulated age errors demonstrating the effect of sampling pattern, number of sampling points and "analysis" errors on age results. The three colors in the 100×100 grid indicate the “analytical error” due to counts of ^{206}Pb.

Fig. 3 Schematic illustration of the Brama software workflow. The software flow runs from top to bottom.

Fig. 4 Diagram of the Brama interface and functional zones. Zones 1 and 2 are for importing data; Zone 3 is for bias correction calculation, setting of analysis and filter parameters; Zone 4 is for Bayesian regression; Zones 5 and 6 are for multi-file processing and mapping; Zone 7 is for information display.

Fig. 5 Regression result of age and common Pb using Brama (a) and Tera-Wasserburg plots on calcite dating by LA-ICP-MS (b) data not filtered; (c) data rejection of low U-count areas; (d) filtered data with SWD (square of weighted deviations) < 10) and (e) spatial distribution of U and Pb isotope counts.

Fig. 6 Regression results of age and common Pb using Brama Bayesian and Tera-Wasserburg plots for apatite dating by LA-ICP-MS. When U/Pb is not dispersed, only reliable ages are obtained by Bayesian or Tera-Wasserburg methods (a, b). When U/Pb is dispersed, both reliable ages and common Pb can be obtained (c-d).

View Article Online
DOI: 10.1039/D2JA00341D

Fig. 1

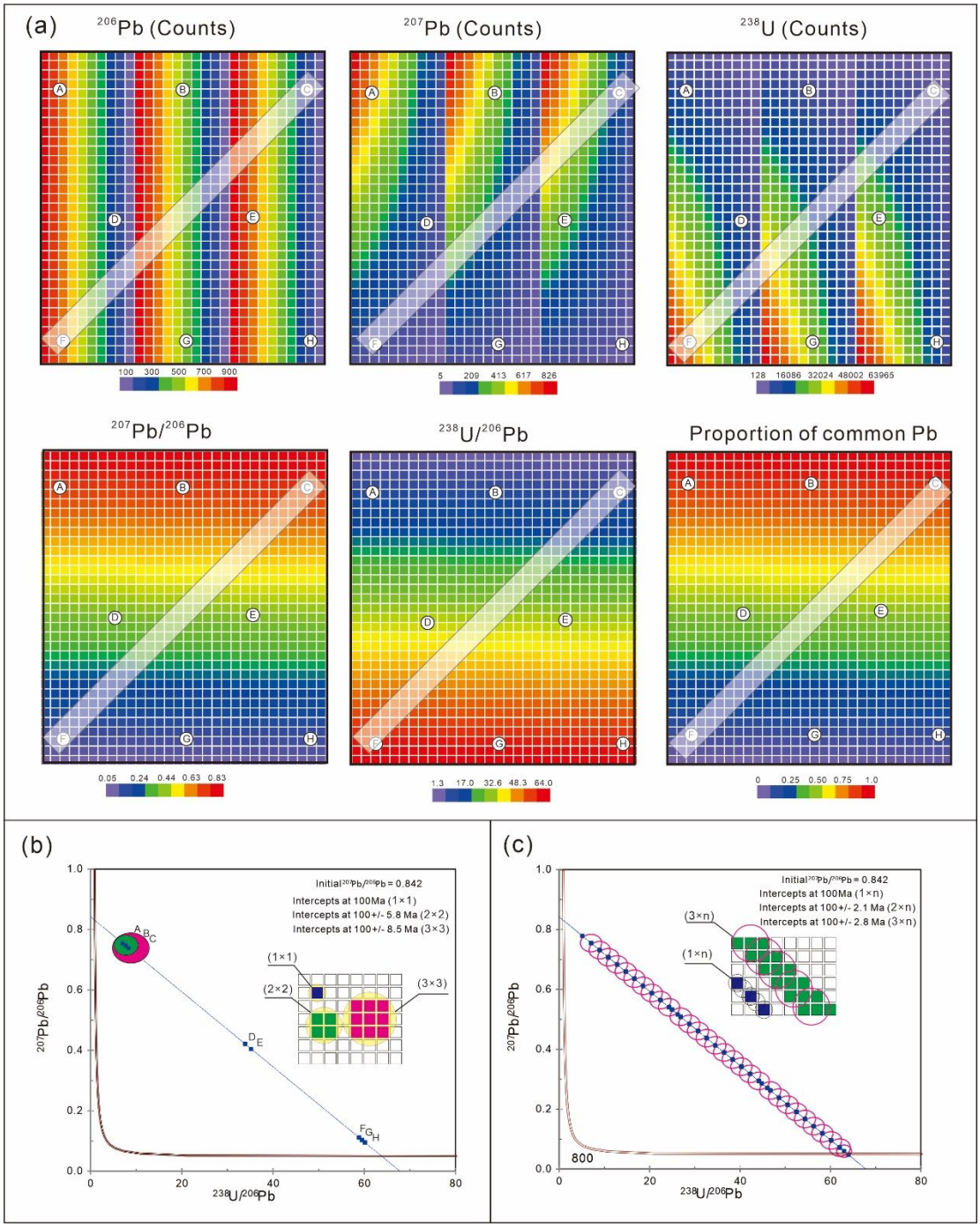

View Article Online
DOI: 10.1039/D2JA00341D

Fig. 2

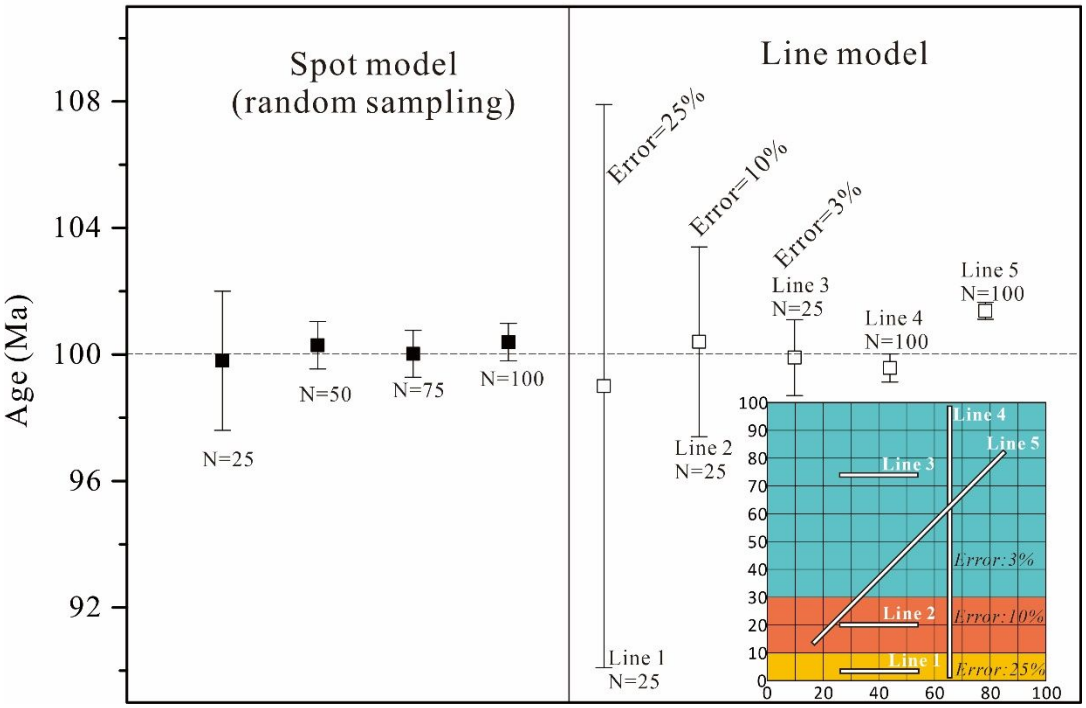

View Article Online
DOI: 10.1039/D2JA00341D

Fig. 3

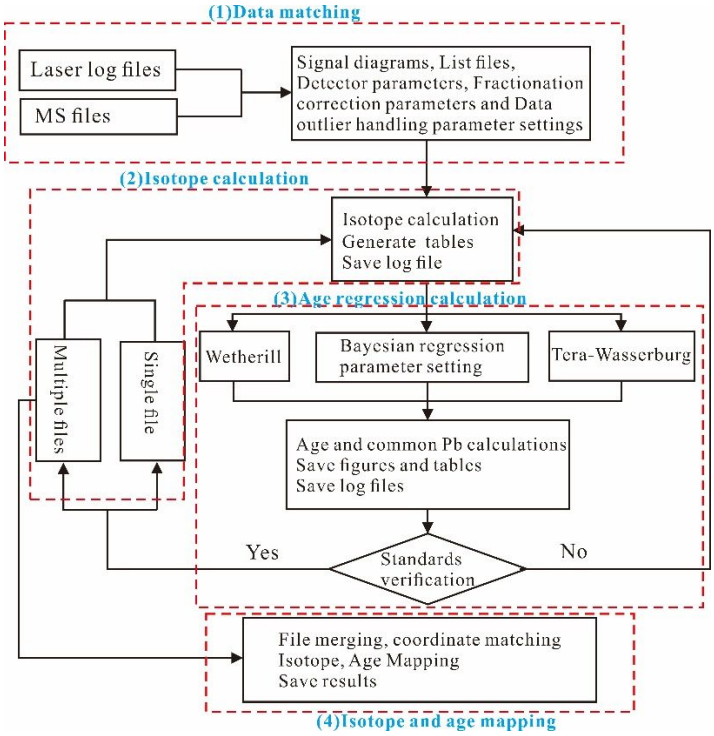

View Article Online
DOI: 10.1039/D2JA00341D

Fig. 4

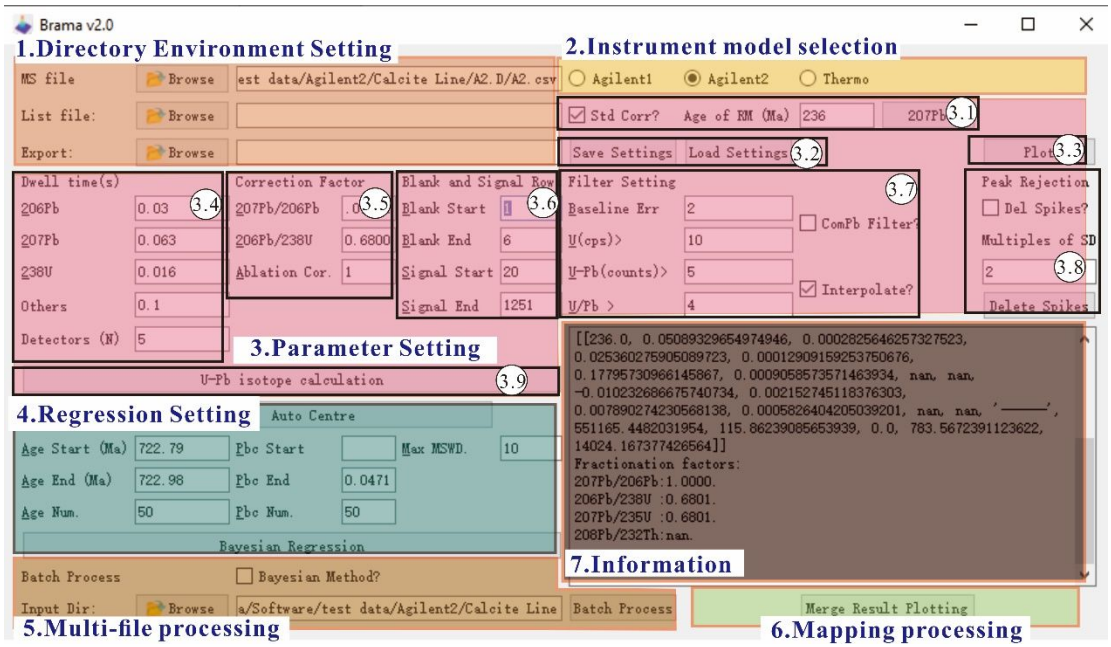

View Article Online
DOI: 10.1039/D2JA00341D

Fig. 5

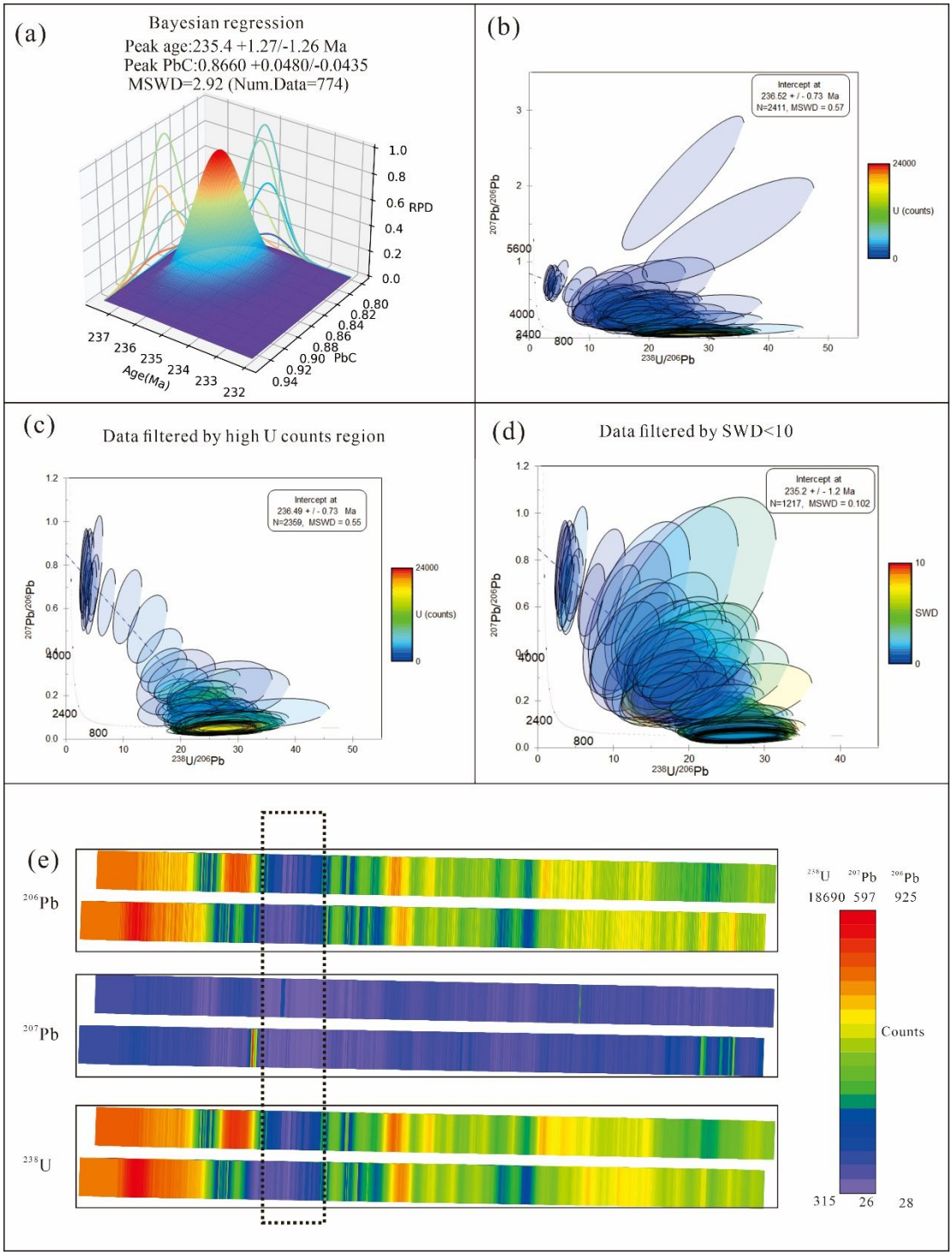

View Article Online
DOI: 10.1039/D2JA00341D

Fig. 6